Flight Trajectory Simulation of Fluid Payload Projectiles

Harold R. Vaughn,* Walter P. Wolfe,† and William L. Oberkampf‡
Sandia National Laboratories, Albuquerque, New Mexico

A flight trajectory simulation method has been developed for calculating the six degree of freedom motion of fluid filled projectiles. Numerically calculated internal fluid moments and experimentally known aerodynamic forces and moments are coupled to the projectile motion. Comparisons of predicted results with flight test data of an M483 155 mm artillery projectile with a highly viscous payload confirm the accuracy of the simulation. This simulation clearly shows that the flight instability is due to the growth of the nutation component of angular motion caused by the viscous effects of the fluid payload. This simulation procedure, when used in conjunction with the previously developed method for calculating internal fluid moments, allows the designer to examine the effects of various liquid payloads and container geometries on the dynamic behavior of flight vehicles.

Nomenclature

a	= cylinder radius
A_1	= α component of K_1
A_2	= α component of K_2
B_1	= β component of K_1
B_2	= β component of K_2
cSt	= centiStoke = 10^{-6}m^2/s
d	= body diameter
$\vec{F}$	= force vector
F_N	= total normal force
F_x, F_y, F_z	= force components
g	= acceleration of gravity
$\tilde{I}$	= moment of inertia tensor
$I_{xx}, I_{yy}, I_{zz}, I$	= moment of inertia components
K_1	= nutation angle
K_2	= precession angle
K_3	= trim angle
K_4	= yaw of repose angle
m	= mass of body
$\vec{M}$	= moment vector
M	= total pitch moment
M_x, M_y, M_z	= moment components
M_α	= $(\partial M/\partial\alpha)_{\alpha=0}$
p	= spin rate of body
p^*	= spin rate of body axis system
q	= pitch rate of body
q^*	= pitch rate of body axis system
QE	= quadrant elevation
r	= yaw rate of body
r^*	= yaw rate of body axis system
R_a	= Reynolds number based on radius
t	= time
T	= air temperature
u, v, w	= velocity components
$\vec{V}$	= velocity vector of body
V_s	= speed of sound
x, y, z	= axes for fixed plane coordinate system
X_E, Y_E, Z_E	= earth fixed axes
α	= angle of attack
α_t	= total angle of attack
$\tilde{\alpha}$	= transient component of angle of attack
β	= angle of sideslip
$\tilde{\beta}$	= transient component of angle of sideslip
θ_n	= nutation angle
Θ	= Euler angle-pitch
Θ_f	= filtered value of Euler angle-pitch
ν	= kinematic viscosity
ρ	= air density
τ	= dimensionless spin rate
ϕ_a	= aerodynamic roll angle
Φ	= Euler angle-roll
Ψ	= Euler angle-yaw
Ψ_f	= filter value of Euler angle-yaw
$\vec{\omega}$	= rotation vector of body
ω_n	= nutation rate of body
ω_s	= spin rate of body
ω_x	= spin rate of axis system
ω_1	= nutation rate of body
ω_2	= precession rate of body
$\vec{\Omega}$	= rotation vector of reference axes

Superscript

$(\dot{\ })$	= derivative with time = d/dt

Introduction

In 1976 a new 155 mm artillery projectile (XM761), which contained a nonrigid payload consisting of cotton wicks and white phosphorus in a cylindrical canister, demonstrated rapid despin and flight instability when the phosphorus was in a liquid state.[1] Although the immediate problem was solved by severely restricting the motion of the fluid, the cause of the problem remained obscure because the internal fluid motion is extremely difficult to analyze. Analytical efforts, such as those by Murphy[2] and Herbert,[3] have concentrated on developing a basic understanding of the internal fluid flow. They have improved the understanding of the problem but suffer from simplifying assumptions required to sove such a complex problem.

Vaughn, Oberkampf, and Wolfe[4,5] achieved a numerical solution for the internal flow of a viscous fluid in a spinning, nutating cylinder. A steady-state, finite difference solution was obtained to the incompressible, three-dimensional, Navier-Stokes equations in a nutating aeroballistic coordinate system. The fluid induced roll and yaw moments calculated by this procedure agreed well with the moments measured by Miller.[1]

In the present work, the six degree of freedom flight dynamics equations are developed that couple the vehicle motion with the combined effects of the fluid induced moments

Received July 12, 1985; presented as Paper 85-1824 at the AIAA Atmospheric Flight Mechanics Conference, Snowmass, CO, Aug. 19-21, 1985; revision received Nov. 4, 1985.

*Supervisor, Aeroballistics Division. Associate Fellow AIAA.
†Member of Technical Staff, Aeroballistics Division. Senior Member AIAA.
‡Member of Technical Staff, Aeroballistics Division. Associate Fellow AIAA.

and external aerodynamic forces and moments. A procedure has been developed that implements these equations and calculates the dynamic behavior of fluid filled vehicles. To verify the accuracy of this trajectory simulation method, trajectories are calculated for 155 mm artillery projectiles with liquid payloads and compared with flight test data.

Internal Fluid Moment Calculations

The numerical method previously developed by Vaughn, Oberkampf, and Wolfe[4,5] computes the fluid motion inside a spinning, nutating canister. This numerical method solves the three-dimensional Navier-Stokes equations in cylindrical coordinates using Chorin's artificial compressibility method.[6] An iterative finite difference procedure was used to obtain solutions for highly viscous fluids; 0.9×10^4 to 1.0×10^9 centiStokes (cSt). The fluid motion calculated by this method is a function of three independent parameters; spin rate, ω_s, nutation rate, ω_n, and nutation angle, θ_n. The axis system used for the fluid moment calculations is shown in Fig. 1. This is a noninertial, nonspinning, nutating, aeroballistic axis system. It should be noted that standard aeroballistic axes used in flight dynamics do not spin or nutate. The present fluid moment axes have a rotation rate, relative to inertial space, equal to the nutation rate. In this coordinate system, the solution is steady-state for constant ω_s, ω_n, and θ_n. It is assumed in the present work that these steady-state solutions adequately represent the fluid motion for a projectile in flight that has precession, slowly varying spin and nutation rates, and a slowly varying nutation angle. The calculated fluid moments are due to the deviation of the fluid motion from solid body rotation ($a\omega_s$). The pitch moment of a solid body whose mass is equal to that of the fluid must be accounted for separately from the fluid moments.

An M483 155 mm projectile containing a liquid payload has been carefully flight tested by D'Amico and Clay[7] (round no. BRL-E1-9542). For this projectile the liquid container was a cylinder with a radius of 2.18 in. and a length of 19.617 in. The cylinder was completely filled with corn oil at a viscosity of 1.7×10^5 cSt. Numerical calculations for the fluid moments acting on this container were made as a function of nutation angle, nutation rate, and spin rate. Values for these parameters are the following: θ_n or $K_1 = 5$, 10, 15, 20, 30, 40, 50, 70, and 90 deg; ω_n or $\omega_1 = 200$, 400, 600, 800, 1000, 1200, 1600, and 2000 rpm; and $\omega_s = 1000$, 2000, 3000, 4000, 6000, 10000, 14000, and 18000 rpm. This matrix required calculations for some 576 sets of conditions. The symbols θ_n and ω_n were used previously[4,5] in the development of the fluid calculation method and are equivalent to K_1 and ω_1 used in tricyclic theory.[8,9]

It is noted that the present matrix of solutions is given in terms of the dimensional variables of the problem. For the fixed container dimensions and given fluid in the present problem, the following nondimensional parameters have been suggested[2,3] to characterize the flow field and resulting liquid moments:

$$K_1 = \text{nutation rate}$$

$$\tau = \frac{\omega_1}{\omega_s + \omega_1 \cos K_1} = \text{dimensionless spin rate}$$

$$R_a = \frac{(\omega_s + \omega_1 \cos K_1)a^2}{\nu} = \text{Reynolds number based on total spin rate and container radius}$$

Even if these parameters correctly characterize the problem, they do not reduce the number of numerical solutions needed in the present flight simulation. This is because each combination of nutation angle, nutation rate, and spin rate given above produces a unique combination of K_1, τ, and R_a.

A number of the combinations of K_1, ω_1, and ω_s for which liquid moments were calculated do not occur in the flight of liquid filled projectiles. This broad range of solutions were calculated, however, in order to document the variation of each of the moments with these parameters. These solutions should be useful in evaluating approximate analytical techniques. A detailed discussion and listings of these calculated fluid moments can be found in Ref. 10.

Flight Dynamics Equations of Motion

Before the equations of motion are written for a six-degree of freedom (DOF) simulation, careful consideration must be given to the choice of an axis system. The two axis systems most commonly used in the published literature are the body fixed axis system and the aeroballistic axis system. In the body fixed axis system, the axes are rigidly attached to the body and, therefore, undergo all of the motions and accelerations of the body. In the aeroballistic axis sytem, the axes undergo all motions of the body with the exception of roll. The roll rate of the aeroballistic axes is zero. Depending upon the implementation and information desired from the 6-DOF simulation, each of these axis systems has its advantages and disadvantages. For the present effort neither of these axis systems was chosen because a direct comparison between the simulated dynamic motion and flight test yawsonde data could not be made.

The axis system chosen for the present 6-DOF simulation is a fixed plane axis system shown in Fig. 2. In this axis system, the axes undergo all of the motions of the body with the exception of roll. Unlike the aeroballistic axes, however, these axes can have a nonzero roll rate. It is, therefore, imperative that one distinguish between p, the roll rate of the body, and p^*, the roll rate of the axis system. Relative to inertial space, the orientation of these fixed plane axes is defined by two Euler

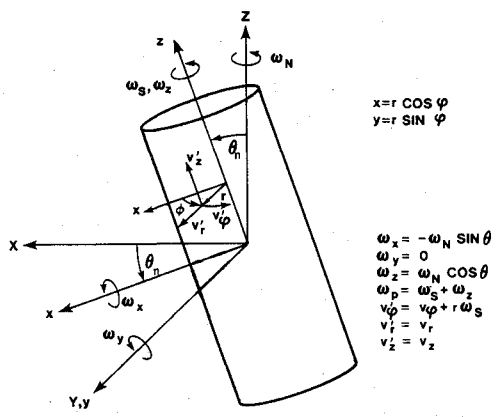

Fig. 1 Fluid moment axis system.

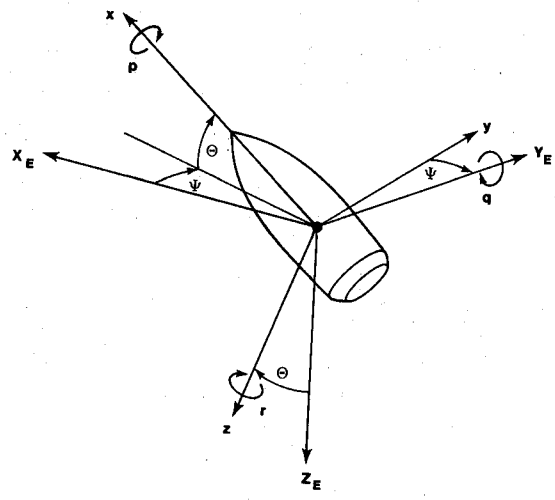

Fig. 2 Fixed plane axis system.

angles, Ψ and Θ. The third Euler angle Φ is identically equal to zero. The roll rate experienced by these axes is that which is necessary to keep $\Phi \equiv 0$. This axis system was chosen because the x-z plane is always perpendicular to the Earth's surface (the X_E-Y_E plane). This means that the output of this simulation is directly comparable to flight test yawsonde data. These axes also facilitate the incorporation of the moments induced by the fluid payload. For the purposes of this simulation, it is assumed that the Earth fixed axes (X_E-Y_E-Z_E) form an inertial reference frame, i.e., the Earth is flat and nonrotating. For the purposes of the simulations discussed in this work, this is a valid assumption. This work examines the angular behavior of the body and compares with flight test yawsonde data. These experimental data are measured relative to the sun line, not the Earth's surface, and are, therefore, independent of the Earth's rotation.

Vaughn[8] has previously shown that the vector form of the moment equation can be written as

$$\vec{M} = \tilde{I}\dot{\vec{\omega}} + \dot{\tilde{I}}\,\vec{\omega} + \vec{\Omega} \times \tilde{I}\vec{\omega}, \tag{1}$$

where $\tilde{I}$ is the moment of inertia tensor, $\vec{\omega}$ is the rotation vector of the body, and $\vec{\Omega}$ is the rotation vector of the reference axes. In the present work, it is assumed that $\tilde{I}$ is constant in time ($\dot{\tilde{I}} \equiv 0$), that all cross products of inertia are zero, and that the body is symmetrical in both the pitch and yaw planes ($I_{yy} = I_{zz} = I$). Equation (1) can then be written in scalar form as

$$M_x = I_{xx}\dot{p} + q^* r I - q r^* I \tag{2}$$

$$M_y = I\dot{q} + p r^* I_{xx} - p^* r I \tag{3}$$

$$M_z = I\dot{r} + p^* q I - p q^* I_{xx}. \tag{4}$$

For the fixed plane axis system shown in Fig. 2, both the axes and the body have the same pitch and yaw rate, i.e., $q = q^*$ and $r = r^*$. The axes and body do not, however, have the same roll rate, i.e., $p \neq p^*$. Letting $\omega_x = p^*$, Eqs. (2-4) can be reduced to

$$M_x = I_{xx}\dot{p} \tag{5}$$

$$M_y = I\dot{q} + r(pI_{xx} - \omega_x I) \tag{6}$$

$$M_z = I\dot{r} + q(\omega_x I - pI_{xx}) \tag{7}$$

Solving Eqs. (5-7) for the angular accelerations gives

$$\dot{p} = M_x / I_{xx} \tag{8}$$

$$\dot{q} = \{r(\omega_x I - pI_{xx}) + M_y\}/I \tag{9}$$

$$\dot{r} = \{q(pI_{xx} - \omega_x I) + M_z\}/I \tag{10}$$

Etkin[11] and Ashley[12] write the vector form of the force equation as

$$\vec{F} = m(\mathrm{d}\vec{V}/\mathrm{d}t + \vec{\omega} \times \vec{V}) \tag{11}$$

where $\vec{V}$ is the velocity of the center of mass of the body and m is the mass. In scalar form, Eq. (11) can be wirtten as

$$F_x - mg\sin\Theta = m(\dot{u} + qw - rv) \tag{12}$$

$$F_y = m(\dot{v} + ru - \omega_x w) \tag{13}$$

$$F_z + mg\cos\Theta = m(\dot{w} + \omega_x v - qu). \tag{14}$$

Solving for the accelerations gives

$$\dot{u} = rv - qw - g\sin\Theta + F_x/m \tag{15}$$

$$\dot{v} = \omega_x w - ru + F_y/m \tag{16}$$

$$\dot{w} = qu - \omega_x v + g\cos\Theta + F_z/m. \tag{17}$$

The remainder of the equations needed to form a closed set are the expressions for the rates of change of Euler angles and the body's velocity components expressed in the Earth fixed coordinate system. These expressions are derived in any text on flight mechanics[11,12] and will be presented here without derivation. Referenced to the Earth fixed axes, the velocity equations are

$$\dot{X}_E = u\cos\Theta\cos\Psi - v\sin\Psi + w\sin\Theta\cos\Psi \tag{18}$$

$$\dot{Y}_E = u\cos\Theta\sin\Psi + v\cos\Psi + w\sin\Theta\sin\Psi \tag{19}$$

$$\dot{Z}_E = -u\sin\Theta + w\cos\Theta \tag{20}$$

The rates of change of Euler angles are given by

$$\dot{\Theta} = q \tag{21}$$

$$\dot{\Psi} = r\sec\Theta \tag{22}$$

$$\dot{\Phi} = \omega_x + r\tan\Theta \tag{23}$$

Since $\dot{\Phi} \equiv 0$, Eq. (23) gives

$$\omega_x = -r\tan\Theta \tag{24}$$

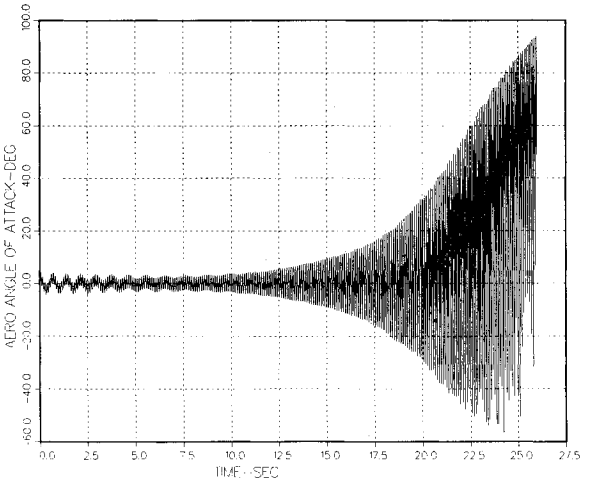

Fig. 3 Aerodynamic angle of attack.

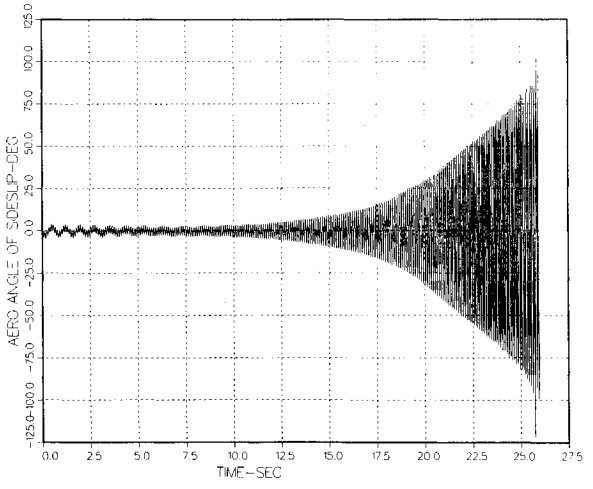

Fig. 4 Aerodynamic angle of sideslip.

Six-Degree of Freedom Simulation

External Aerodynamic Characteristics

Equations (8-10) and (15-24), together with the numerical method for computing payload induced moments, form a closed set of equations that describe the motion of a flight vehicle in the fixed plane coordinate system shown in Fig. 2. These equations have been incorporated into a six degree of freedom trajectory simulation code that can be used to analyze the dynamic behavior of fluid filled projectiles. The roll, pitch, and yaw moments applied to the body during flight are a combination of aerodynamic and fluid payload induced moments. This trajectory code accounts for both of these contributions.

For the present 6-DOF simulation, aerodynamic force and moment coefficients are functions of Mach number and total angle of attack α_t. Damping coefficients are functions of Mach number only. All of the aerodynamic coefficients are entered into the code in tabular form. Linear interpolation is used to determine the values at the appropriate Mach number and total angle of attack.

Once the aerodynamic forces and moments are determined in the plane of the total angle of attack, they are resolved into components in the planes of the aerodynamic angle of attack α and angle of sideslip β. These angles are calculated by

$$\alpha = \tan^{-1}\frac{w}{u} \tag{25}$$

$$\beta = \tan^{-1}\frac{v}{u} \tag{26}$$

$$\alpha_t = \tan^{-1}\frac{\sqrt{v^2+w^2}}{u} \tag{27}$$

In order to resolve the forces and moments into their proper components, the angle between the plane of α_t and the plane of α must be known. This angle, designated the aerodynamic roll angle ϕ_a, is defined by

$$\tan\phi_a = v/w \tag{28}$$

The forces and moments in the α and β planes are then given by

$$F_z = -F_N\cos\phi_a \tag{29}$$

$$F_y = -F_N\sin\phi_a \tag{30}$$

$$M_y = M\cos\phi_a \tag{31}$$

$$M_z = -M\sin\phi_a \tag{32}$$

where F_N is the total normal force and M the total pitch moment.

Computational Procedure

The magnitudes of the four components of coning motion (nutation, precession, trim, and yaw of repose) are represented by the symbols K_1, K_2, K_3, and K_4, respectively. The angular rate of each component is represented by ω_1, ω_2, and p, respectively. Figures 3 and 4 show the aerodynamic angles of attack and sideslip calculated from Eqs. (25) and (26) for a typical simulated flight of a fluid filled projectile. These curves show the presence of the different modes of angular motion. In the first few seconds of flight, one can readily discern the higher frequency nutation superimposed over the lower frequency precession. As the flight progresses, the precession damps out and has disappeared by approximately 10 s. Conversely, the nutation motion grows with time and is totally dominant after approximately 7 s. Above approximately 20 s, the presence of the yaw of repose mode of motion is indicated by the shift of the angle of attack envelope toward more positive values. The magnitude of the yaw of repose is larger than for solid payload projectiles due to the interaction of fluid and aerodynamic forces and moments with the gyroscopic effects. The trim component of motion is small and can be ignored.

As described previously, the computed fluid moments are functions of spin and nutation only. Therefore, in order to determine the fluid moments throughout the flight, the nutation component (K_1 and ω_1) must be isolated from the total angular motion. Tricyclic theory provides a set of equations that may be used to isolate the angular motion components of a projectile with a rigid internal payload. One must be very careful, however, in attempting to use these equations for a fluid filled projectile because of the restrictions inherent in the theory. Tricyclic theory is based on a solution to a linear differential equation that inherently has the assumptions of constant coefficients and small angles of attack. Also, the theory does not include any effects of the fluid induced moments. Because of the restrictions, tricyclic equations can only be used for the first portion of a flight where both the angle of attack and the fluid moments are small.

The numerical procedure used to separate the nutation from the total angular motion begins by processing the calculated values of pitch and yaw Euler angles. The average values of these angles represent the yaw of repose component of motion. If one subtracts these average values from the total motion, the resulting motion contains only nutation and precession. Such an approach is accomplished by the following procedure.

The first step in obtaining K_1 and ω_1 is the use of two-stage, low-pass, Butterworth filter[13] that has a cutoff frequency below the value of the precession frequency ω_2. A two-stage Butterworth filter was chosen because of its sharp cutoff characteristics and small phase lag. This filtering process removes the higher frequency K_1 and K_2 components of motion leaving only the average value of trajectory angles and the low frequency yaw of repose component. Both the yaw and pitch Euler angles Ψ and Θ are processed through this filter. The differences between Ψ and Θ and their filtered values are the transient components of the aeroballistic angles of attack and sideslip. These values are given by

$$\tilde{\alpha} = \Theta - \Theta_f \tag{33}$$

$$\tilde{\beta} = -(\Psi - \Psi_f)\cos\Theta_f \tag{34}$$

The term $\cos\Theta_f$ is present in Eq. (34) because Ψ is measured at $\Theta = 0$ and $\tilde{\beta}$ is measured at $\Theta = \Theta_f$.

The procedure for separating the nutation and precession components is divided into two phases, one for small angles of

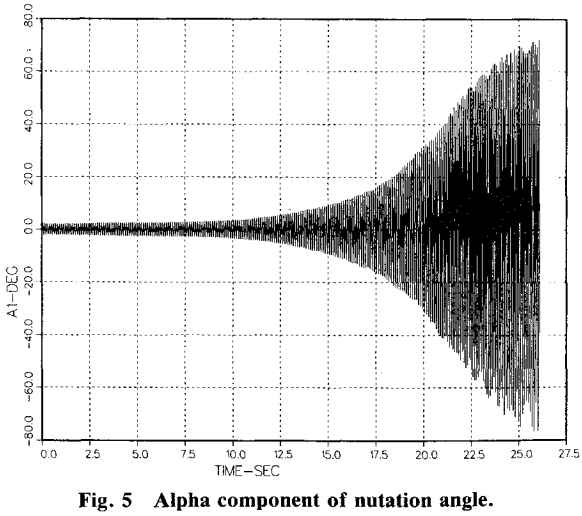

Fig. 5 Alpha component of nutation angle.

attack and one for large angles. For $\alpha_t \leq 10$ deg, equations from tricyclic theory are used. From Ref. 8, the equations for the frequency and magnitude of the K_1 and K_2 components of motion are

$$\omega_1 = \frac{pI_{xx}}{2I} + \sqrt{\left(\frac{pI_{xx}}{2I}\right)^2 - \frac{M_\alpha}{I}} \tag{35}$$

$$\omega_2 = \frac{pI_{xx}}{2I} - \sqrt{\left(\frac{pI_{xx}}{2I}\right)^2 - \frac{M_\alpha}{I}} \tag{36}$$

$$A_1 = -\left(\frac{\dot{\tilde{\beta}} + \omega_2 \tilde{\alpha}}{\omega_1 - \omega_2}\right) \tag{37}$$

$$B_1 = \left(\frac{\dot{\tilde{\alpha}} - \omega_2 \tilde{\beta}}{\omega_1 - \omega_2}\right) \tag{38}$$

$$A_2 = -\left(\frac{\dot{\tilde{\beta}} + \omega_1 \tilde{\alpha}}{\omega_2 - \omega_1}\right) \tag{39}$$

$$B_2 = \left(\frac{\dot{\tilde{\alpha}} - \omega_1 \tilde{\beta}}{\omega_2 - \omega_1}\right) \tag{40}$$

where A and B are the α and β components of K_1 and K_2. K_1 is computed from

$$K_1 = \sqrt{A_1^2 + B_1^2} \tag{41}$$

Above a total angle of attack of 10 deg, it is assumed that the precession has damped to zero and the coning motion is totally due to nutation. Examination of Figs. 3 and 4 shows that this is a valid assumption. K_1 is then determined from

$$K_1 = \sqrt{\tilde{\alpha}^2 + \tilde{\beta}^2} \tag{42}$$

ω_1 is determined by computing the period of the cyclic oscillations of $\tilde{\alpha}$ and $\tilde{\beta}$.

The results of the above procedure are shown in Figs. 5 and 6. These figures show the α and β components of K_1 for the present example case. Comparison with Figs. 3 and 4 shows that the precession component has been removed leaving only nutation.

The moments induced upon the projectile by the fluid payload are calculated in the 6-DOF code from tabular data using linear interpolation at each integration time step to determine the fluid moment for any given K_1, ω_1, and ω_s. The value of the spin rate needed to determine the fluid moment is that measured in the axis system shown in Fig. 1, not in the 6-DOF axis system shown in Fig. 2. This value of spin rate is determined by

$$\omega_s = p - \omega_1 \cos K_1 \tag{43}$$

Within the code, the equations of motion are integrated using a fourth order Runge-Kutta integrator with a fixed time step of 2×10^{-4} s. This time step provides a minimum of 200 steps per pitch cycle for the highest nutation frequency.

The atmospheric model used in this simulation is a simple analytical formulation developed by NACA[14] that is sufficient for the computation of projectile trajectories. The equations for this model are

$$\rho = 0.00238\ [1 + (Z_E/145366)]^{4.2555} \tag{44}$$

$$T = 518.4 + 0.00356617 Z_E \tag{45}$$

The temperature T in °R is used to compute the speed of sound in ft/s from

$$V_s = \sqrt{(1.4)(1716)T} \tag{46}$$

Results

Transonic Launch

In order to verify the accuracy of the six degree of freedom simulation, calculations were made for a fluid filled M483 155 mm projectile that was flight tested by D'Amico and Clay[7] (round no. BRL-E1-9542). Launch conditions were a muzzle velocity of 1089 ft/s (331.6 m/s), a quadrant elevation angle (Q. E.) of 30 deg, and an altitude of sea level. The initial angle and angular rate conditions at the muzzle are unknown and

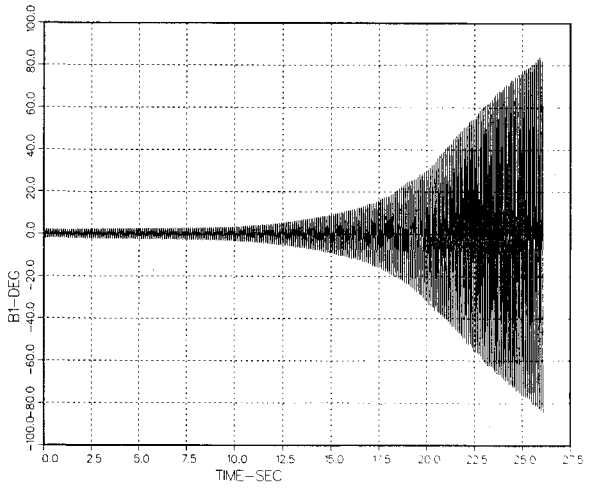

Fig. 6 Beta component of nutation angle.

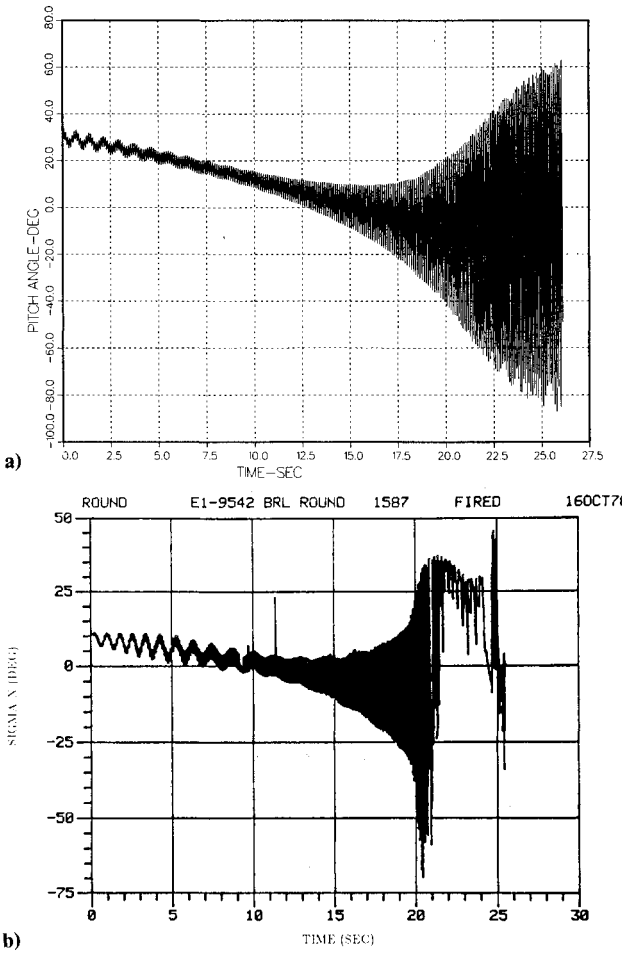

Fig. 7 Comparison of calculated and flight test pitch angle: a) calculated pitch angle, b) experimental pitch angle from Ref. 7.

are difficult to determine for purposes of simulation. There are four possible components involved: α, β, q, and r. Because of the constraints imposed by a launch tube, the initial angles of attack and sideslip are very small. For this simulation it is was assumed that $\alpha=\beta=0$. Examination of the early angle of attack data from D'Amico and Clay[7] with the aid of tricyclic equations shows that $q\approx 0$ and that r must be negative. Calculations were made with r varying between -1 and -2 rad/s. It was found that the effect of varying initial conditions over this range simply shifted the time of occurrence of the instability by a few seconds without appreciably changing the character of the instability. The value of $r=-1.94$ rad/s provided the best match with the flight behavior.

The calculated pitch angle Θ is compared in Fig. 7 with the yawsonde data, SIGMA N, from the flight test. SIGMA N is the angle of the projectile centerline relative to the sun direction. The SIGMA N data must be shifted upward approximately 20 deg to be equal to the true pitch angle. The agreement between the present prediction and experiment is quite good for the entire flight. Both the calculated and experimental data show the decay of the lower frequency precession mode and the growth of the higher frequency nutation mode. The experimental data show a slight growth of the precession prior to the decay. This growth is not present in the computed results. Prior to 21 s, the calculated growth of the nutation mode is approximately equal to the experimental data. The data from the yawsonde are lost when the coning angle reaches 50 deg, which is a limitation of the instrument. The 6-DOF calculation terminates when the pitch angle reaches -90 deg because of a numerical singularity caused by the circular trigonometric functions.

The spin rate for the 6-DOF calculation and the flight data are compared in Fig. 8. The calculations accurately predict the dramatic despin behavior. This figure shows a steady decline in the spin rate from the initial value of approximately 110 Hz to 85 Hz at 20 s. At this time there is a rapid despin to 35 Hz at 25 s. This rapid despin is due to the growth of the liquid despin moment that results from the rapid growth of the nutation angle.

The calculated values of the high frequency nutation component of the motion are compared with flight test data in Fig. 9. Again, they are in good agreement. The simulation accurately predicts the rapid growth of K_1 at approximately 14 s. At 20 s, both the calculation and experimental data show $K_1\approx 30$ deg. The experimental curve shown in Fig. 9 shows that at $t=0$, $K_1=0$, whereas the calculated curve shows that $K_1\approx 2$ deg. The experimental curve in Fig. 9 shows data that were reduced from the original experimental data shown in Fig. 7. Conversations with D'Amico indicate that, because there are no data prior to $t=0$, the reduction process starts with $K_1=0$ at $t=0$. If one extrapolates the envelope of the oscillations in Fig. 7 from $t=5$ s to $t=0$, it is apparent that $K_1\approx 1$-2 deg.

The precision of the agreement of calculations with the flight data depends to a significant extent on the accuracy of the aerodynamic data at high angles of attack ($\alpha>20$ deg). Both static and dynamic aerodynamic coefficients for the M483 were available for angles of attack up to 88 deg, however, the accuracy of the data at these high angles is unknown. The fact that the flight test data and the 6-DOF simulation agree well is strong evidence that both the aerodynamic coefficients and the fluid payload moments are reasonably accurate.

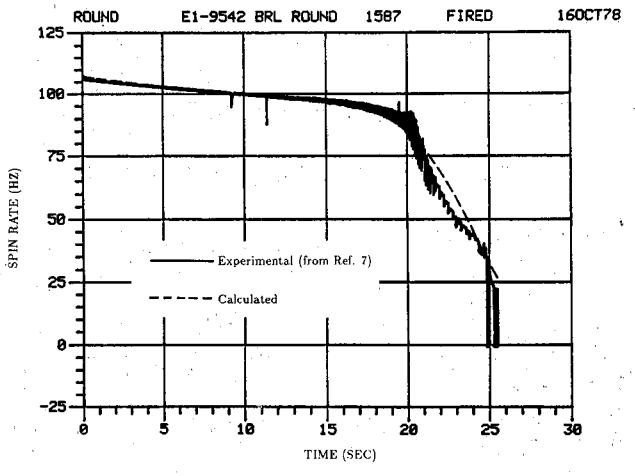

Fig. 8 Comparison of calculated and flight test spin rate.

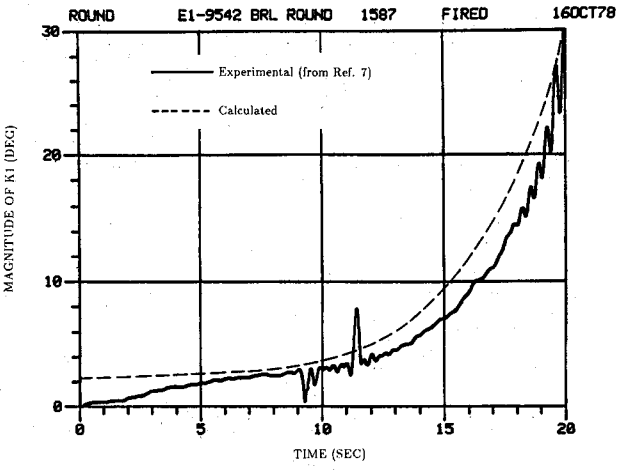

Fig. 9 Comparison of calculated and flight test nutation angle.

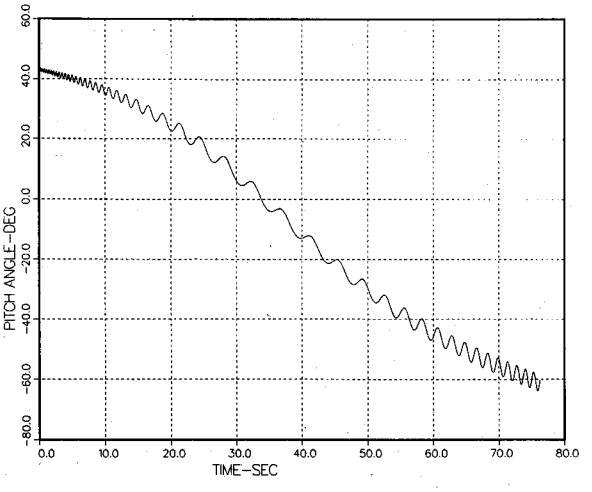

a)

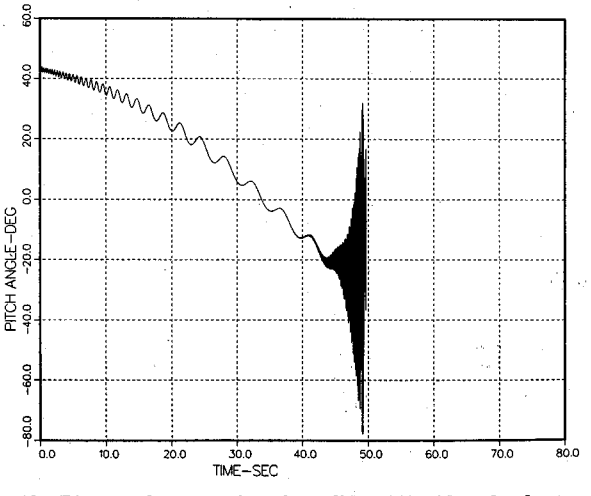

b)

Fig. 10 Pitch angle comparison for solid and liquid payloads at maximum range simulation: a) solid payload; b) liquid payload.

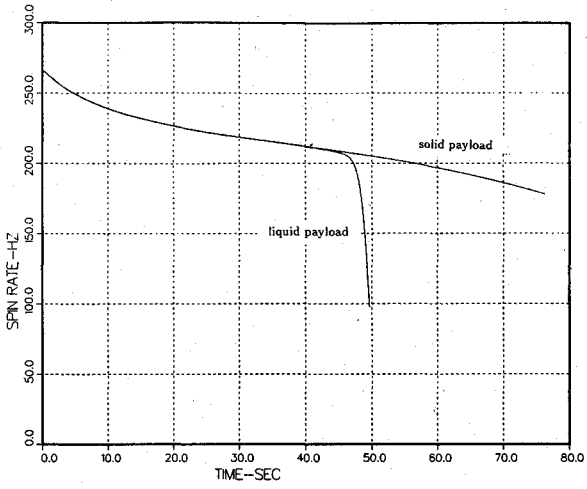

Fig. 11 Spin rate comparison for solid and liquid payloads at maximum range simulation.

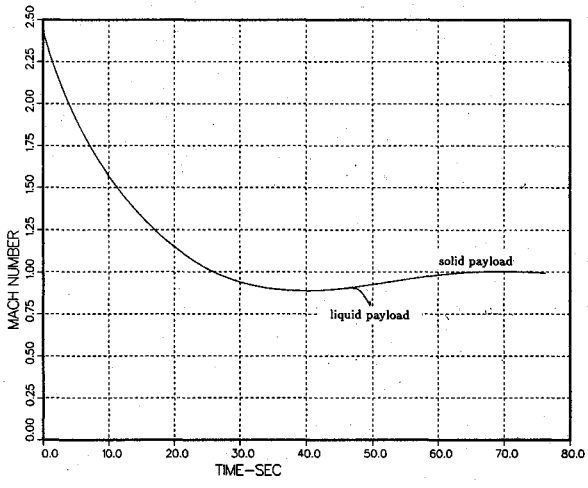

Fig. 12 Mach number comparison for solid and liquid payloads at maximum range simulation.

Supersonic Launch

A flight simulation was made for a maximum range trajectory of the M483. Figures 10-12 show pitch angle (Θ), spin rate, and Mach number, respectively, for both solid and liquid payloads launched at an angle of 43 deg (750 mil) and a muzzle velocity of 2710 ft/s (826 m/s). For the first 40 s of flight, these figures show no discernible difference between the flight of the solid and liquid payloads. Figure 10 shows only the presence of the precession (K_2) component of motion during this time. At approximately 40 s the nutation (K_1) component begins to grow, with the growth becoming very rapid at approximately 45 s. This rapid growth of pitch angle coincides with the rapid decrease in spin rate shown in Fig. 11. There is a very rapid despin from approximately 205 Hz at 45 s to 100 Hz at 49 s. Figure 12 shows that the Mach number at this time is approximately 0.88. Because of the increased drag of the projectile due to the high pitch angle, the Mach number decreases as the instability grows.

These figures show that the fluid projectile experiences a normal, stable flight while the speed remains supersonic. The instability starts when the shell has decelerated into the high subsonic region. At this point the projectile is near apogee where the dynamic pressure is at a minimum and the pitch damping coefficient is about one-third of the supersonic value. The pitch damping moment tends to reduce the nutational amplitude while the fluid yaw moment tends to increase the nutational amplitude. This rapid loss in pitch damping allows the rapid growth in nutation. This type of behavior has

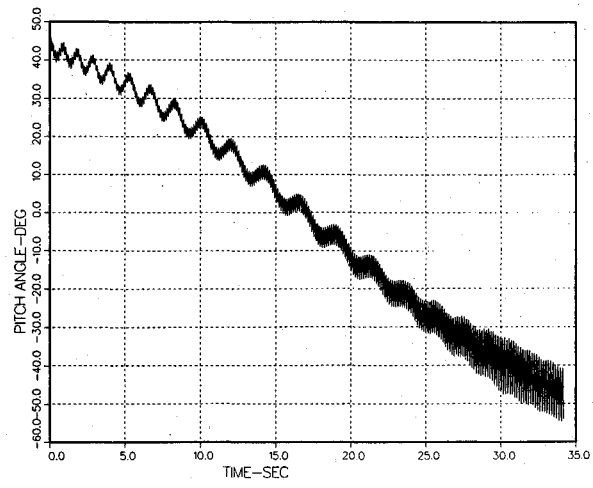

Fig. 13 Pitch angle for subsonic launch simulation.

also been experimentally observed by D'Amico.[15] This implies that at supersonic speeds the aerodynamic stability is sufficient to overcome the destabilizing fluid moments. The growth in the instability occurs at transonic speeds where the aerodynamic stability is reduced to the point that it is less than the fluid instability.

Subsonic Launch

The same trends noted above are also present in a subsonic launch of a fluid filled projectile. The pitch history for a launch at $V = 850$ ft/s and Q.E. = 45 deg is shown in Fig. 13. It can be seen that the nutation rate starts growing immediately but does not diverge as rapidly as that for the higher velocity launches. Because both the nutation and spin rates are smaller than for a transonic launch, the projectile experiences smaller destabilizing fluid moments and, therefore, slower divergence. This translates, in turn, into smaller fluid induced moments. Even though the fluid moments are reduced for this launch, they are still large enough to destabilize the projectile.

Conclusions

A six-degree of freedom trajectory simulation method has been developed that uses numerically calculated fluid moments and complete aerodynamic forces and moments. Comparisons of predicted results with flight test data of an M483 155 mm projectile with a highly viscous payload confirm the accuracy of the simulation. This simulation clearly shows that the flight instability is due to the growth of the nutation component of angular motion caused by the viscous effects of the fluid payload. The instability results when the aerodynamic stability is reduced to the point where the fluid moments predominate. This situation typically occurs in the transonic speed range and when the aerodynamic forces and moments are small due to low dynamic pressure.

Numerical experimentation has shown that the initial angular rate conditions imposed at the muzzle have the effect of shifting the time at which the instability undergoes rapid growth. The initial conditions do not affect the character of the instability. Nominal initial yaw rates of -1 to -2 rad/s gave good results for the current simulation.

The numerical method of calculating the fluid moments appears to be sufficiently accurate for the trajectory simulations. The good agreement with experimental measurements indicate that the internal fluid motion responds rapidly to changes in nutation angle, nutation rate, or spin rate and that the steady-state assumption made in applying the calculated fluid moments to a flight vehicle is valid. This simulation method, when used in conjunction with the previously developed method for calculating internal fluid moments, allows the designer to examine the effects of various liquid payloads and container geometries on the dynamic behavior of flight vehicles.

Acknowledgment

This work was jointly supported by the United States Department of Energy under contract DE-AC04-76DP00789 and the Chemical Research and Development Center (CRDC), United States Army Armament, Munitions, and Chemical Command (AMCCOM), under Military Interdepartmental Purchase Request Number 4311-1424, April 23, 1984. The contracting officer for CRDC was Mr. Miles Miller, Chief, Aerodynamics Research and Concepts Assistance Branch, Research Directorate. The aerodynamic coefficients used in the M483 simulation were supplied by Mr. Miller.

References

[1]Miller, M. C., "Flight Instabilities of Spinning Projectiles Having Nonrigid Payloads," *Journal of Guidance and Control*, Vol. 5, March-April 1982, pp. 151-157.

[2]Murphy, C.H., "Angular Motion of a Spinning Projectile with a Viscous Liquid Payload," Ballistic Research Laboratory Memo Rept ARBRL-MR-03194, Aug. 1982.

[3]Herbert, T., "The Flow of Highly Viscous Fluid in a Spinning and Nutating Cylinder," *Proceedings of the 1983 Scientific Conference on Chemical Defense Research,* Chemical Research and Development Center, Rept. SP-8404, pp. 617-624.

[4]Vaughn, H. R., Oberkampf, W. L., and Wolfe, W. P., "Numerical Solution for a Spinning, Nutating, Fluid-Filled Cylinder," Sandia National Laboratories, Albuquerque, NM, SAND83-1789, Dec. 1983.

[5]Vaughn, H. R., Oberkampf, W. L., and Wolfe, W. P., "Fluid Motion Inside a Spinning, Nutating Cylinder," *Journal of Fluid Mechanics,* Vol. 150, Jan. 1985, pp. 121-138.

[6]Chorin, A. J., "A Numerical Method for Solving Incompressible Viscous Flow Problems," *Journal of Computational Physics,* Vol. 2, Aug. 1967, pp. 12-26.

[7]D'Amico, W. P. and Clay, W.H., "High Viscosity Liquid Payload Yawsonde Data for Small Launch Yaws," Ballistic Research Laboratory Memo. Rept. ARBRL-MR-03029, June 1980.

[8]Vaughn, H. R., "A Detailed Development of the Tricyclic Theory," Sandia National Laboratories, Albuquerque, NM, SC-M-67-2933, Feb. 1968.

[9]Vaughn, H. R., and Wilson, G. G., "Yaw of Repose on Spinning Shells," Sandia National Laboratories, Albuquerque, NM, SC-RR-70-155, Jan. 1970.

[10]Vaughn, H. R., Wolfe, W. P., and Oberkampf, W. L., "Six Degree of Freedom Simulation of Fluid Payload Projectiles Using Numerically Computed Fluid Moments," Sandia National Laboratories, Albuquerque, NM, SAND85-1166, June 1985.

[11]Etkin, B., *Dynamics of Flight*, John Wiley and Sons, Inc., New York, 1959, pp. 94-117.

[12]Ashley, H., *Engineering Analysis of Flight Vehicles,* Addison-Wesley Publishing Company, Reading, MA, 1974, pp. 27-39.

[13]Stearns, S. D., *Digital Signal Analysis*, Hayden Book Co., Inc., Rochelle Park, NJ, 1975, pp. 183-193.

[14]"Notes and Tables for Use in the Analysis of Supersonic Flow," NACA Tech. Note 1428, Dec. 1947.

[15]D'Amico, W. P., "Field Tests of the XM761: Second Diagnostic Test," Ballistic Research Laboratory, Memo. Rept. ARBRL-MR-02806, Jan. 1978.